



Recapture probability for antitrapped Rydberg states in optical tweezers

R. J. P. T. de Keijzer ^{*}, O. Tse, and S. J. J. M. F. Kokkelmans 

*Department of Applied Physics and Eindhoven Hendrik Casimir Institute,
Eindhoven University of Technology, P.O. Box 513, 5600 MB Eindhoven, The Netherlands*



(Received 16 March 2023; accepted 26 July 2023; published 24 August 2023)

In a neutral-atom quantum computer, the qubits are individual neutral atoms trapped in optical tweezers. Excitations to Rydberg states form the basis for the entanglement procedure that is at the basis of multiqubit quantum gates. However, these Rydberg atoms are often antitrapped, leading to decoherence and atom loss. In this work, we give a quantum-mechanical description of the antitrapping loss rates and determine the recapture probability after Rydberg excitation, distinguishing between having the laser traps turned on and off. We find that ample time ($\approx 30 \mu\text{s}$, in a ^{88}Sr system) is needed for the wave functions to expand out of the trap. Therefore, even with traps on, $\approx 100\%$ recapture probabilities can be expected for times in which significant entanglement operations between atoms can be performed. We find that for two-dimensional radial traps with bosonic ^{88}Sr atoms, the time in which perfect recapture can be achieved is of the same order of magnitude for traps turned on and off.

DOI: [10.1103/PhysRevA.108.023122](https://doi.org/10.1103/PhysRevA.108.023122)

I. INTRODUCTION

Neutral atoms trapped in optical tweezers are emerging as a promising platform for scalable quantum computing. The main advantages of these platforms are the demonstrated long coherence time [1], the versatility of the atomic arrangements with conservation of entanglement [2], and, generally, the contemporary advances in laser-cooling techniques for use in atomic clocks, allowing for accurate control of the atoms [3–5]. To construct a quantum computer out of such a system, an array of optical tweezers is created with individual alkali or alkaline-earth atoms trapped inside. A consequentially logical choice is to encode the $|0\rangle$, $|1\rangle$ qubit manifold in the (meta)stable states that make up the atomic clock transition. These states are well isolated from the other atoms and have long lifetimes. For bosonic ^{88}Sr , this is the $^1S_0 \leftrightarrow ^3P_0$ transition, where the metastable state 3P_0 has a lifetime on the order of minutes [1]. Besides these properties, a quantum computing platform has more stringent requirements on the few-particle level, such as single-qubit control and the ability to entangle neighboring atoms.

This entanglement is mediated through auxiliary Rydberg states, which interact via van der Waals interactions [6]. These are electronic structure states of the atom with a high principle quantum number n and have significantly lower lifetimes than the clock states due to losses from, e.g., photoionization, spontaneous emission, and antitrapping from the Rydberg states [7]. This paper will principally analyze the latter, where antitrapping is caused by the fact that polarizability of the Rydberg states switches signs compared to the clock states. The resulting light-atom potential becomes concave, actively repelling the atom [8]. Therefore, minimizing the time that the

atom spends in the Rydberg state is important for optimizing the pulse [9] or gate robustness [7,10].

One strategy to avoid such losses is to switch off the trap for the duration of the entanglement procedure, then switch it back on for recapture [11]. The antitrapping behavior will then be mitigated because the spatial wave function evolves under a free potential instead of a concave inverse Gaussian (i-Gauss) potential (resulting from the Gaussian intensity pattern of the optical tweezers [12]). Nevertheless, the atom still expands under the free potential and eventually leaves the trap after a longer time spent in the Rydberg state [13]. Furthermore, there are other challenges when switching off the trap. The blinking on and off of the traps can lead to additional losses of the atoms in the qubit manifold and thus the entire qubit array. On a sequential gate-based platform, this can severely limit the depth of the gate circuit [11]. One way to avoid these losses is to use interferometrically generated bottle beam traps to trap both the qubit and Rydberg states [14]. However, these are technically challenging to create and generally less deep.

Another possibility is to simply leave the trap on for the Rydberg excitation. It was generally assumed that the antitrapping would lead to an exponential loss in time of the atom [15]. However, recent experiments found that this is not the case [10,11,16,17]. This can be understood as, despite the repulsive potential, the atoms needing an initialization time to start leaving the trap.

In this paper, we shed light on this discussion by researching how recapture probabilities depend on the status of the trap (on or off). The layout of this paper is as follows. Section II describes the theory behind our quantum-mechanical recapture probability model. There, we first look into the relevant timescales in Sec. II A. We then consider the potentials and initial states in Sec. II B. Section II C describes the evolution methods. In Sec. II D we argue that we can infer two-dimensional (2D) results for the trap from our

^{*}Corresponding author: r.j.p.t.d.keijzer@tue.nl

one-dimensional (1D) trap calculations. Section III shows results for recapture probabilities based on the parameters of a realistic ^{88}Sr setup.

II. QUANTUM MODEL OF RECAPTURE PROBABILITIES

In this section, we discuss the underlying evolution equations and approximations necessary to calculate recapture probabilities. Note that our method is a fully quantum mechanical model of recapture probabilities considering tweezer status, whereas semiclassical methods have been considered before [18–20]. In contrast to the semiclassical Monte Carlo methods, our fully quantum method allows us to get a very good analytical expression for the state evolution, greatly simplifying the calculation of recapture probabilities. Furthermore, the quantum-mechanical approach leads to a physically intuitive definition of recapture probability as the overlap between the evolved state and the bound states of the trap. Last, especially where accelerations are involved in the classical setting, the propagator formalism is, particularly under the effect of an external potential, a more accurate method to describe the long-term evolution than the classical dynamics, as it follows the Schrödinger equation under which the atom actually evolves.

A. Relevant timescales

In this section, we analyze the relevant timescales in the recapture probability problem. When an atom is excited to the Rydberg state, four timescales play a role (Fig. 1). First, we consider the excitation time $\tau_{\text{spin}} = 1/\Omega_R$, with Ω_R being the Rabi frequency. This is the timescale determining how fast one can excite an atom from the qubit manifold to the Rydberg state. In contrast, the motional time $\tau_{\text{mot}} = 1/\omega$, with ω being the trap frequency, which is the trap motional time determining the speed of evolution of motional states. In current ^{88}Sr setups, $\Omega_R \approx 10$ MHz and $\omega \approx 20$ –60 kHz [12,15,21,22], showing that the excitation can be considered instantaneous in the timescale of motional development. Therefore, the motional state will not evolve significantly during the excitation from the qubit manifold. Second, we consider the interaction time $\tau_{\text{int}} = 1/V = -R^6/C_6$, where C_6 is the van der Waals coefficient and R is the interatomic distance defined by the tweezer lattice spacing, and the time in which we recapture with $\approx 100\%$ certainty τ_{recap} (see Eq. (10)). When making quantum state preparations, it is important that a large part of the Hilbert space can be reached, meaning that maximally entangled states should also be achievable [23]. Thus, in the Rydberg state, we want to be able to perform sufficient entanglement between the neighboring atoms in the platform, as controlled by τ_{int} . Thus, we want recapture time $\tau_{\text{recap}} \gg \tau_{\text{int}}$.

B. Potentials and initial states

The potential an atom experiences in a Gaussian optical tweezer in cylindrical coordinates (r, z) is given by

$$U(r, z) = \frac{U_0}{1 + z^2/z_R^2} \exp\left(\frac{-2r^2}{w_0^2(1 + z^2/z_R^2)}\right), \quad (1)$$

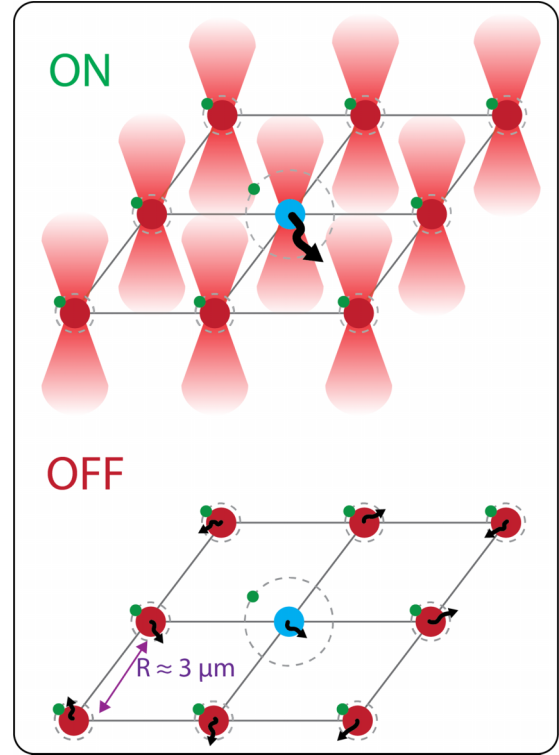


FIG. 1. A 3×3 grid of optical-tweezer traps with interatomic separation R of the order of a few micrometers. The middle atom is excited to the Rydberg state (blue), while all other atoms stay in the qubit manifold (red). With the traps turned on, the excited atom is actively forced outwards as the tweezer potential becomes repulsive for the Rydberg state. The rest of the atoms stay trapped. With the traps off, the drift will be less. However, all atoms expand in that case

where w_0 is the laser beam waist, z_R is the Rayleigh range, and the maximal potential $U_0 = -\alpha_0 I_0 / 2c\epsilon_0$ [24]. Here, $I_0 = 2P/\pi w_0^2$ is the central intensity of the laser beam, where P is the total power of the laser. Furthermore, α_v is the polarizability of state $|v\rangle$ [25] given by

$$\alpha_v(\omega_{\text{laser}}) = \frac{2}{3(2J+1)} \sum_n \frac{(E_n - E_v) |\langle v|D|n\rangle|^2}{(E_n - E_v)^2 - \omega_{\text{laser}}^2},$$

where J is the angular momentum of $|v\rangle$, E_i is the energy of state $|i\rangle$, D is the electric dipole operator, and ω_{laser} is the frequency of the laser beam. The polarizability characterizes a state's susceptibility to an electric field. For alkali atoms and highly excited states, polarizabilities can be determined using an atomic structure library [26]. For low-energy states of alkaline-earth metals, such as ^{88}Sr , one needs to resort to more complex methods because of the presence of two or more valence electrons. In this work, we use the methods described in work by Safronova *et al.* [27,28] to calculate polarizability values.

We consider a ^{88}Sr -based quantum computer using the states forming the clock transition, $5s^2 1S_0$ and $5s5p^3 P_0$, as our qubit states. For these states, a magic wavelength has been identified at 813.4 nm, where the polarizabilities of both states are equal to 287 a.u. [27]. Operating the traps at a

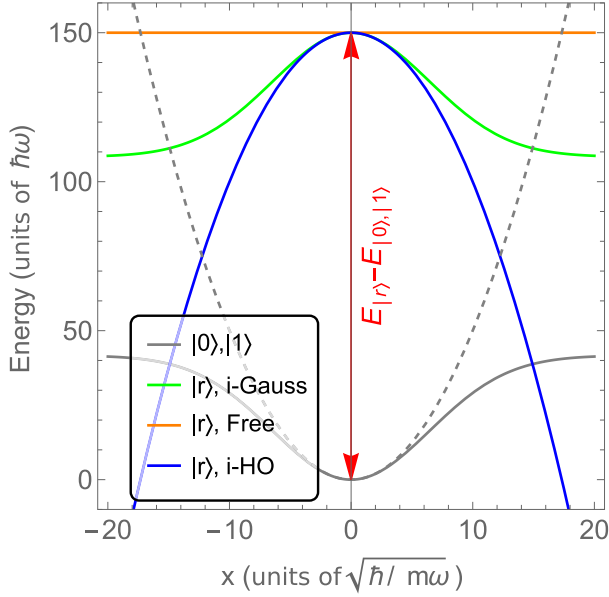


FIG. 2. Potentials experienced by the qubit manifold states $|0\rangle$ and $|1\rangle$ and the Rydberg state $|r\rangle$ and their (inverse) harmonic oscillator approximations valid for small $|x|$. The difference in state-related energies $E_{|r\rangle} - E_{|0\rangle, |1\rangle}$ is not to scale

magic wavelength is preferable, as it eliminates phase buildup between the qubit states due to ac Stark shifts. For the Rydberg state in ^{88}Sr , we find a polarizability of the same magnitude but different sign [17]. Thus, the Rydberg state experiences an inverted potential compared to the qubit states when the laser is turned on, as illustrated in Fig. 2. Even when the laser is turned off and the atom subsequently experiences no potential, the wave function expands under the free-particle propagator. This means that when an atom is excited to the Rydberg state, it eventually leaves the trap and can no longer be recaptured when it is deexcited back to the qubit manifold. In the rest of this section we describe our model for calculating recapture probabilities when we excite an atom from the qubit manifold to the Rydberg state, let the wave function expand for a set time t , and deexcite it back to the qubit manifold.

Since recapture is sensitive to only radial motion [20,29], only the radial directions of the trap are considered; we thus take $z = 0$. Furthermore, in Sec. II D, we argue that we can infer the 2D (radial) recapture probabilities from 1D results. In the rest of this section, we thus consider a 1D optical tweezer trap. Based on Eq. (1), we consider

$$\begin{aligned} V_{\text{HO}}(x) &= \frac{1}{2}m\omega^2 x^2, & V_{\text{Free}}(x) &= 0, \\ V_{\text{Gauss}}(x) &= -U_0 + U_0 \exp(-2x^2/w_0^2), \end{aligned} \quad (2)$$

for the harmonic oscillator (HO), Gauss, and free potentials, respectively. We also define $V_{i\text{-HO}} = -V_{\text{HO}}$ and $V_{i\text{-Gauss}} = -V_{\text{Gauss}}$ for the inverse HO (i-HO) and inverse Gauss potentials. The harmonic oscillators in this case are approximations to the Gaussian potentials for small $|x|$ and are often used as such (see Fig. 2). Using the approximation $\exp(y) \approx 1 + y$ in

Eq. (3), the values of ω are related to U_0 , z_R , and w_0 as

$$\omega_{x,y} = \sqrt{\frac{4|U_0|}{mw_0^2}}, \quad \omega_z = \sqrt{\frac{2|U_0|}{mz_R^2}}. \quad (3)$$

When the atom is in the Rydberg state, its wave function $|\psi(x, t)\rangle$ evolves under the time-dependent 1D Schrödinger equation as

$$\begin{aligned} i\hbar\partial_t|\psi(x, t)\rangle &= -\frac{\hbar^2}{2m}\partial_{xx}|\psi(x, t)\rangle + V(x)|\psi(x, t)\rangle, \\ |\psi(x, 0)\rangle &= |\psi_0\rangle. \end{aligned}$$

Based on Eq. (3), we transform our coordinates as

$$x \rightarrow \tilde{x}x_0, \quad t \rightarrow \tilde{t}t_0, \quad x_0 = \sqrt{\hbar/m\omega}, \quad t_0 = 1/\omega$$

to give the dimensionless equation

$$\begin{aligned} i\partial_{\tilde{t}}|\psi(\tilde{x}, \tilde{t})\rangle &= -\frac{1}{2}\partial_{\tilde{x}\tilde{x}}|\psi(\tilde{x}, \tilde{t})\rangle + \frac{1}{\hbar\omega}V(\tilde{x})|\psi(\tilde{x}, \tilde{t})\rangle, \\ |\psi(\tilde{x}, 0)\rangle &= |\psi_0\rangle. \end{aligned}$$

For convenience, we drop the tildes on the transformed coordinates. For Gaussian laser traps, we also define the edge of the trap X_{edge} as

$$\frac{V_{\text{Gauss}}(X_{\text{edge}})}{V_{\text{Gauss}}(0)} \approx 0.01 \Rightarrow X_{\text{edge}} \approx 3.035\sqrt{\frac{|U_0|}{\hbar\omega}}. \quad (4)$$

In contemporary ^{88}Sr tweezer setups, trap depths U_0 of several hundred microkelvins can be achieved. However, when exciting atoms to the Rydberg state, the traps are often adiabatically lowered to minimize trap scattering (which is especially important in ^{88}Sr) and to increase the recapture probability [12].

As the atoms in the trap are cooled close to the ground state, the initial state of the system can be approximated by the density matrix of a quantum harmonic oscillator at temperature T [30], given by

$$\rho_T(0) = \frac{1}{Z} \sum_{n=0}^{\infty} e^{-\beta E_{\text{HO},n}} |\psi_{\text{HO},n}\rangle \langle \psi_{\text{HO},n}|, \quad (5)$$

where $\beta = 1/k_B T$, $E_{\text{HO},n} = \hbar\omega(n + \frac{1}{2})$, $Z = \sum e^{-\beta E_{\text{HO},n}}$, and

$$|\psi_{\text{HO},n}\rangle = \frac{1}{\sqrt{2^n n!}} \left(\frac{m\omega}{\pi\hbar}\right)^{1/4} e^{-\frac{m\omega x^2}{2\hbar}} H_n\left(\sqrt{\frac{m\omega}{\hbar}}x\right)$$

is the n th eigenstate of the HO potential, with H_n being the n th Hermitian polynomial. Let $\rho_T(t)$ evolve under an arbitrary Schrödinger equation with initial state $\rho_{T,0}$, and let $|\psi_{\text{HO},n}(t)\rangle$ denote the solution to this same equation with initial state $|\psi_{\text{HO},n}\rangle$. Then the expectation value of an observable \hat{O} with respect to $\rho_T(t)$ can, by the orthogonality of $|\psi_{\text{HO},n}\rangle$, be calculated as

$$\text{Tr}[\rho_T(t)\hat{O}] = \frac{1}{Z} \sum_{n=0}^{\infty} e^{-\beta E_{\text{HO},n}} \langle \psi_{\text{HO},n}(t) | \hat{O} | \psi_{\text{HO},n}(t) \rangle. \quad (6)$$

We want to excite the atom to the Rydberg state, where it experiences a potential $V_{i\text{-Gauss}}$ (or zero if we switch off the trap) for a time t . After this, we deexcite the atom back to the qubit manifold and determine the Franck-Condon overlap

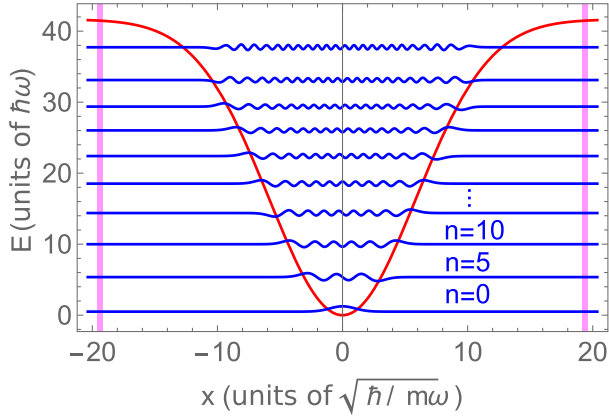


FIG. 3. Potential and approximated eigenvalues for the non-inverted 1D Gauss potential, with $U_0 = 50 \mu\text{K}$ and $\omega = 25 \text{ kHz}$. The edges of the trap are colored in purple. Plotted per five eigenfunctions.

with the bound states of the potential V_{Gauss} [see Eq. (9)]. To do so, we have to determine the bound states $|\psi_{\text{Gauss},n}\rangle$ (of which there are only finitely many, in contrast to the HO potential [31]). We would have to solve the equation

$$-\frac{1}{2}\partial_{xx}|\psi\rangle + \frac{U_0}{\hbar\omega}(1 - e^{-2x^2x_0^2/\omega_0^2})|\psi\rangle = E|\psi\rangle$$

for energies $E < 0$. However, no analytic solution is known for the Gauss potential [32]. As mentioned before, for $|x| \ll 1$, V_{Gauss} resembles V_{HO} . Therefore, we approximate solutions to the normal Gauss potential as linear combinations of harmonic oscillator solutions (see Fig. 3) as

$$|\psi_{\text{Gauss},n}\rangle = \sum_{i=0}^K \alpha_i^{(n)} |\psi_{\text{HO},i}\rangle \quad (7)$$

for some $K \in \mathbb{N}$, $\alpha_i^{(n)} \in \mathbb{C}^K$. As the Gauss potential resembles the HO potential for $|x| \ll 1$ and the energies in the HO potential increase as $E_n = \hbar\omega(n + 1/2)$, $U_0/\hbar\omega$ is a rough estimate of the number of bound states, on which the initial choice of K is based. We note that since there are only finitely many bound states in the Gaussian trap, there is also a finite extent to these bound states, allowing for a value of K at which the approximation in Eq. (7) is very good.

The eigensystem of the non-inverted Gauss Hamiltonian in the basis of the first K eigenstates of the HO is calculated by diagonalizing the matrix \mathcal{A} with matrix elements $[\mathcal{A}]_{m,n} = \langle \psi_{\text{HO},m} | -1/2\partial_{xx} + V_{\text{Gauss}}(x) | \psi_{\text{HO},n} \rangle$. The bound-state approximations are then given by those states with eigenvalues smaller than zero; the eigenvectors correspond to the coefficients $\alpha_i^{(n)}$. For this work, we choose $K > U_0/\hbar\omega$ in such a way that if we increase K even more, the eigenvalues and eigenvectors $\alpha_i^{(n)}$ no longer change significantly.

At low temperatures, the thermalized state in Eq. (9) has significant contributions of only the lowest-energy eigenstates. Therefore, we have to look at the values of

$$\begin{aligned} \frac{Z_N}{Z} &= \frac{\sum_{n=0}^N \exp(-\beta E_n)}{Z} \\ &= 2 \exp\left(-\frac{\hbar\omega(1+N)}{2k_b T}\right) \sinh\left(\frac{\hbar\omega(1+N)}{2k_b T}\right) \end{aligned}$$

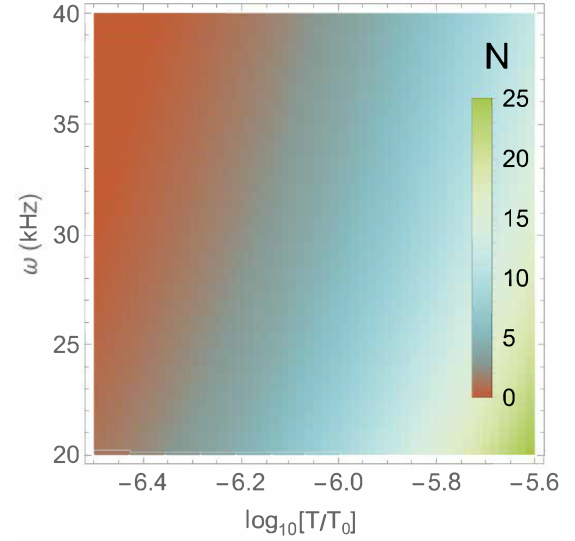


FIG. 4. Levels N at which $Z_N/Z > 0.99$ for varying temperatures T and frequencies ω , with $T_0 = 1 \text{ K}$. For low T and high ω , it is enough to take only the first few HO eigenstates into account for the initial state.

for a decent cutoff of the series expansion. Here, Z_N is the cutoff partition function, quantifying how much of the thermalized state is in the first N levels. For a specific temperature T , we choose our N to be the minimal value such that $Z_N/Z > 0.99$. Figure 4 shows these values of N as a function of T and ω .

C. Propagators and recapture probabilities

With the initial state and bound states defined, the next step is to calculate the evolution of the state under various potentials. The highly dispersive behavior of wave functions under concave potentials [33] makes it difficult to numerically solve the time-dependent Schrödinger equation.

Interestingly enough, analytic propagators exist for the free and i-HO solutions [34], given by

$$\begin{aligned} K_{\text{Free}}(x; x'; t - t') &= \frac{1}{2\pi} \int_{-\infty}^{+\infty} \exp[ik(x - x')] \exp\left(-\frac{i\hbar k^2(t - t')}{2m}\right) dk \\ &= \left(\frac{m}{2\pi i\hbar(t - t')}\right)^{\frac{1}{2}} \exp\left(-\frac{m(x - x')^2}{2i\hbar(t - t')}\right) \end{aligned}$$

for the free Hamiltonian and

$$\begin{aligned} K_{\text{i-HO}}(x; x'; t - t') &= \sqrt{\frac{\omega}{2\pi i\hbar \sinh[\omega(t - t')]}} \\ &\quad \times \exp\left(\frac{i}{\hbar} S(x, t, x', t')\right), \\ S(x, t, x', t') &= \frac{\omega[\cosh[\omega(t - t')](x^2 + x'^2) - 2xx']}{2 \sinh[\omega(t - t')]} \end{aligned}$$

for the Hamiltonian with the inverse HO potential.

For $|\psi(x, 0)\rangle = |\psi_{\text{HO},0}(x)\rangle$, this gives

$$|\psi_{\text{Free}}(x, t)\rangle = -\frac{(-1)^{3/4}}{\pi^{1/4}\sqrt{t-i}} \exp\left(\frac{ix^2}{2(t-i)}\right),$$

$$|\psi_{\text{i-HO}}(x, t)\rangle = \pi^{-1/4}\Gamma(t)^{-1/2} \exp\left(\frac{iS(x, t, 0, 0)}{\hbar}\right) \\ \times \exp\left(-\frac{i\omega}{2\hbar\sinh(\omega t)}\frac{x^2}{\Gamma(t)}\right),$$

$$\Gamma(t) = \cosh(\omega t) + i\frac{\hbar}{\omega}\sinh(\omega t).$$

Expressions for other initial states can be constructed similarly. In the literature, one often defines the survival probability $P_{\text{init}}(t)$ [35,36] as

$$P_{\text{init}}(t) := |\langle\psi(t)|\psi_0\rangle|^2,$$

i.e., the overlap with the initial state at time t . One can show that at $t = 0$, its first derivative is equal to zero (see Appendix B). Looking at the second derivative at $t = 0$ then gives an indication of the decay rate under a certain potential. Because the potentials are time independent, this quantity intuitively dictates the rate of atom loss within the high-recapture-probability regime, which is the regime we are interested in. We call this term $\dot{P}_{\text{init},V}(0)$ the *initial quantum spread* under potential V . The expression for this is derived in Appendix B and is given by

$$\dot{P}_{\text{init},V}(0) = -2\text{Cov}_{\psi_0}\left(V - \frac{1}{2}\frac{\partial^2}{\partial x^2}, V - \frac{1}{2}\frac{\partial^2}{\partial x^2}\right). \quad (8)$$

We can further extend this idea to looking at the overlap with all bound states, called the *recapture probability*:

$$P_{\text{recap}}(t) := \sum_{n=0}^N |\langle\psi(t)|\psi_{\text{Gauss},n}\rangle|^2, \quad (9)$$

which can be interpreted as the probability of recapturing the atom in the trap after deexciting it back to the qubit manifold after it has evolved for a time t . Using the analytic expressions for $|\psi(t)\rangle$ and the HO approximation of the bound states as in Eq. (7), we can calculate $P_{\text{recap}}(t)$ analytically with the integral expression given in Appendix A. We want to define τ_{recap} as the maximal time spent in the Rydberg state, for which we almost certainly recapture the atom. Based on Eq. (9), we define

$$\tau_{\text{recap}} := \max_{t>0} P_{\text{recap}}(t) > 1 - 10^{-4}, \quad (10)$$

where the 4 in the exponent is taken to match recently achieved fidelity figures for single-qubit gates in Rydberg architectures [4,37,38].

D. Two-dimensional considerations

Having defined the model for a 1D trap, the radial 2D case needs to be considered. When looking at the 2D case, the following approximation can be made. If the trap is deep enough, the trap can be approximated as a 2D Harmonic oscillator, where the x and y directions are independent, and the bound states factor as $|\psi_{\text{Gauss},n_1,n_2}(x, y)\rangle = |\psi_{\text{Gauss},n_1}(x)\rangle |\psi_{\text{Gauss},n_2}(y)\rangle$ by separation of variables. If the expanding

TABLE I. Parameters used in the simulation and calculations.

Parameter	Symbol	Value	Units	Ref.
Trap frequency	ω	25	kHz	[11,12]
Trap depth	U_0	50	μK	[12,21]
Mass	m	87.90	amu	
Temperature	T	730	nK	[12,21]
van der Waals coefficient	C_6/\hbar	-154	$\text{GHz}/\mu\text{m}^6$	[15]
Interatomic distance	R	3	μm	[12,22]

wave function also were to factor as $|\psi_{2\text{D}}(x, y, t)\rangle = |\psi_{1\text{D}}(x, t)\rangle |\psi_{1\text{D}}(y, t)\rangle$, then the recapture probability would become

$$P_{\text{recap},2\text{D}}(t) = \sum_{n_1,n_2} |\langle\psi_{2\text{D}}(t)|\psi_{\text{Gauss},n_1,n_2}\rangle|^2 \\ = \sum_{n_1} |\langle\psi_{1\text{D}}(t)|\psi_{\text{Gauss},n_1}\rangle|^2 \\ \times \sum_{n_2} |\langle\psi_{1\text{D}}(t)|\psi_{\text{Gauss},n_2}\rangle|^2 \\ = P_{\text{recap},1\text{D}}(t)^2.$$

Clearly, the bound functions of the 2D case do not exactly factor as such, as a combination of a barely unbound state in x with a deep bound state in y can still have negative energy and thus be bound. Furthermore, the x and y axes are not entirely independent since a state's projections on the x and y axes might be individually bound but the total state can be unbound because it extends significantly in a diagonal direction. However, as the wave function extends quickly when reaching the end of the trap, we hypothesize that this approximation is valid for deep traps. To verify this, we also solve the 2D Schrödinger equation in radial coordinates as

$$i\partial_t |\psi(r, \phi, t)\rangle = -\frac{1}{2}\Delta_{r,\phi} |\psi(r, \phi, t)\rangle + V(r) |\psi(r, \phi, t)\rangle,$$

$$\Delta_{r,\phi} = \left[\frac{1}{r} \frac{\partial}{\partial r} \left(r \frac{\partial}{\partial r} \right) + \frac{1}{r^2} \frac{\partial^2}{\partial \phi^2} \right].$$

Bound states for the 2D Gaussian are constructed, like in the 1D case, as linear combinations of radial 2D HO solutions given by

$$|\psi_{\text{HO},n,l}(r, \phi)\rangle = \frac{1}{\sqrt{2\pi}} \sqrt{\frac{2\alpha!}{(\alpha+|l|)!}} e^{-\frac{r^2}{2}} r^{|l|} L_{\alpha}^{(|l|)}(r^2) e^{il\phi},$$

where $l \in \{-2n, -2n+2, \dots, 2n\}$, $\alpha = (n - |l|)/2$, and $L_{\alpha}^{(|l|)}$ is the generalized Laguerre polynomial. We always assume a radial initial wave function such that the evolved state $|\psi(t)\rangle$ does not have an angular dependence at all times t . Therefore, we need to calculate only the overlap with bound states that also do not have an angular dependence. If the initial wave function does have a radial dependence (for instance, because of nonzero temperatures) the results will not change significantly as thermalized states are considered [see Eq. (6)] and the overlaps and energy differences for angular excited states do not differ substantially from the radially symmetric states [see Eq. (A1)].

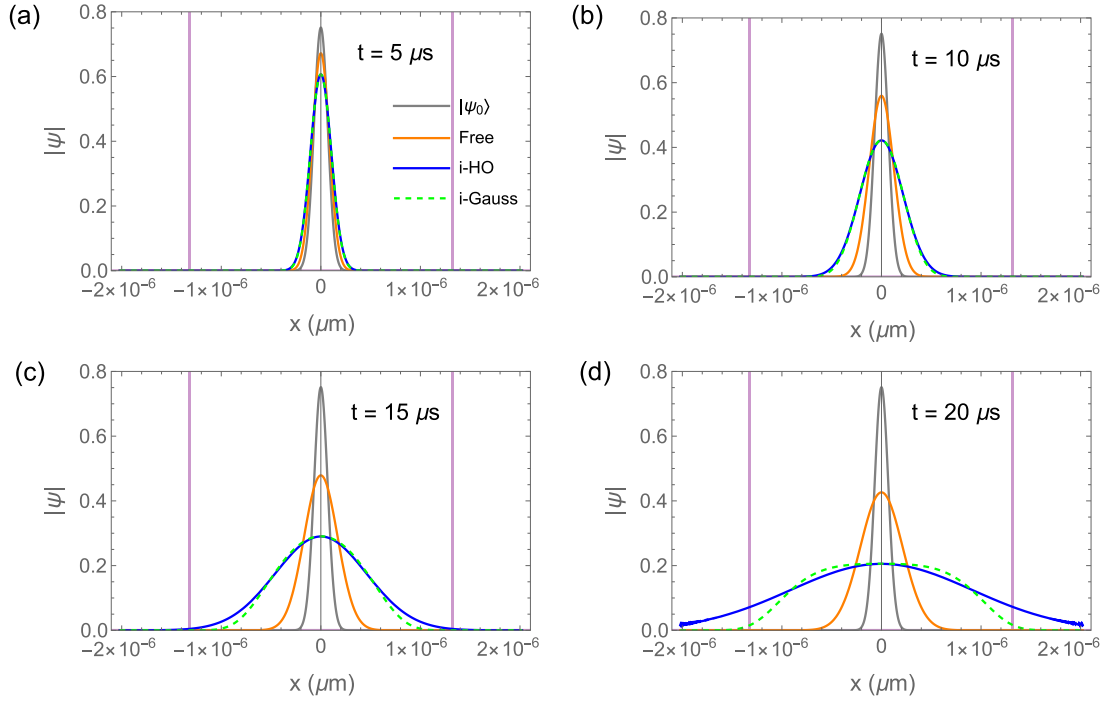


FIG. 5. Evolution of the $|\psi(x, 0)\rangle = |\psi_{\text{HO},0}\rangle$ initial state for different 1D potentials, with $U_0 = 50 \mu\text{K}$ and $\omega = 25 \text{ kHz}$. For times $t < 15 \mu\text{s}$ the i-HO approximation agrees with the i-Gauss solution. Once the atoms start leaving the trap, numerical errors start to occur [see edges of (d)], and the i-HO approximation is no longer valid. The edges of the trap are indicated in purple.

III. RESULTS

This section shows results for the recapture probabilities of atoms for tweezers turned on and off and varying tweezer parameters. In all calculations, we use the parameter values given in Table I [11,12,15,21,22] unless specified otherwise. From these parameters, we get $\tau_{\text{int}} = 4.7 \text{ ns}$. We desire to have recapture time $\tau_{\text{recap}} \gg \tau_{\text{int}}$.

We construct the bound state for the realistic parameters $U_0 = 50 \mu\text{K}$ and $\omega = 25 \text{ kHz}$, which gives $U_0/\hbar\omega \approx 41$, so we take $K = 55$ and find 48 bound states (see Fig. 3) according to the linear approximation method described in Sec. II B. For $n < 10$ we then have $\alpha_n \approx 1$ and thus $|\psi_{\text{Gauss}, n}\rangle \approx$

$|\psi_{\text{HO}, n}\rangle$, showing that the HO eigenfunctions are good approximations of the noninverted Gauss eigenfunctions for these low-lying states.

Figure 5 shows the (numerically calculated) evolution of a 1D $|\psi_{\text{HO},0}\rangle$ initial state under various potentials, with $U_0 = 50 \mu\text{K}$ and $\omega = 25 \text{ kHz}$. We see that the i-HO potential is a good approximation of the i-Gauss evolution for times $t < 15 \mu\text{s}$. Note that numerical errors start to occur at times $t > 20 \mu\text{s}$. This is due to the high dispersivity caused by the concave potentials [33], which makes a Dirichlet or von Neumann boundary problem [39] hard to solve, highlighting the importance of the analytic propagator expressions in Sec. II C.

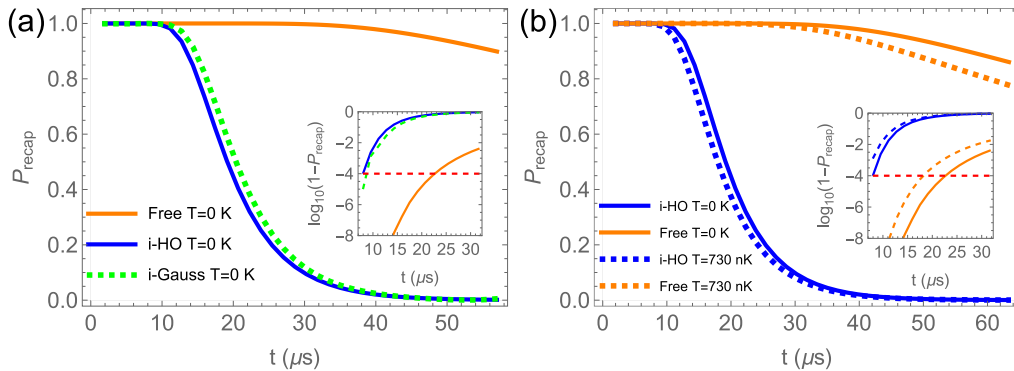


FIG. 6. (a) Recapture probabilities of the 1D free, i-HO, and i-Gauss potentials at $T = 0 \text{ K}$ for $U_0 = 50 \mu\text{K}$ and $\omega = 25 \text{ kHz}$. The free and i-HO values are calculated analytically using the propagators in Sec. II C. The i-Gauss solutions are calculated numerically. The dashed red lines in the insets indicate the recapture probability bound for τ_{recap} . i-HO is seen to be a relatively tight lower-bound approximation of the i-Gauss recapture probabilities. (b) Recapture probabilities of the free and i-HO potentials at $T = 0 \text{ K}$ and $T = 730 \text{ nK}$ for $U_0 = 50 \mu\text{K}$ and $\omega = 25 \text{ kHz}$. Higher temperatures lower the recapture probabilities; however, for realistic temperatures this effect is relatively small.

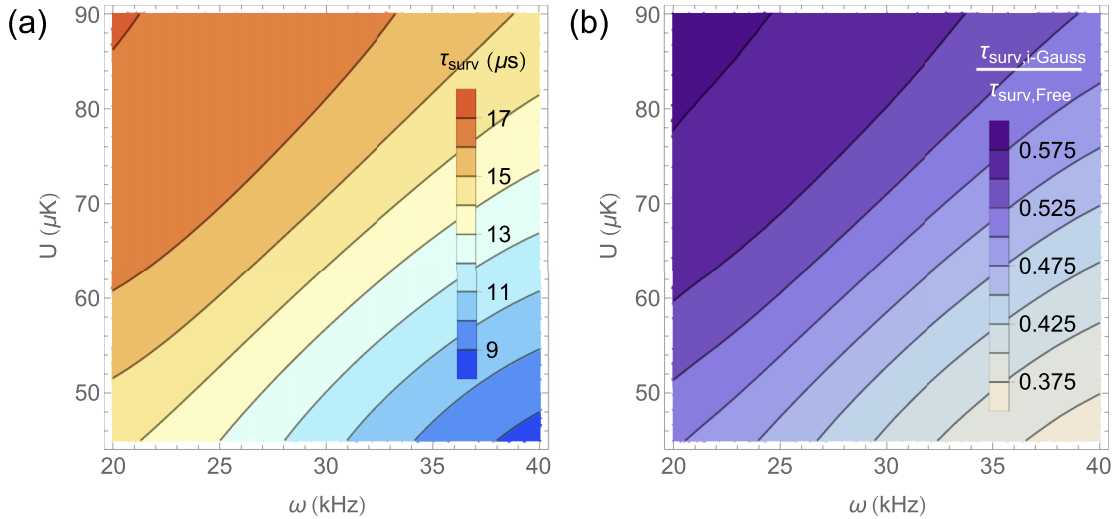


FIG. 7. (a) Recapture times $\tau_{\text{recap,i-Gauss}}$ and (b) recapture time ratio $\tau_{\text{recap,i-Gauss}}/\tau_{\text{recap,Free}}$ for varying U_0 and ω in the 1D case. The recapture times increase with increasing U_0 and decreasing ω_0 . Since contour lines are relatively straight, the ratio U_0/ω and, through Eq. 8, the trap edge X_{edge} can thus be used as predictors of the recapture times. From (b) we note that the recapture times for the i-Gauss potential stay in the same order of magnitude as the free potential.

Figure 6 shows the recapture probabilities of the $U_0 = 50 \mu\text{K}$ and $\omega = 25 \text{ kHz}$ trap for the free, i-HO, and i-Gauss potentials. Note that because of numerical error, the i-Gauss evolution is fully accurate only up to $30 \mu\text{s}$. From this, we again confirm that the i-HO potential is a good approximation to the i-Gauss evolution for low enough evolution times. From Eq. (8), we get initial quantum spreads of $\dot{P}_{\text{init,i-HO}}(0) = -1$ and $\dot{P}_{\text{init,i-Gauss}}(0) = -0.98$. The inset in Fig. 6 indeed confirms these results by showing that the initial loss rates for an i-HO potential are higher than for an i-Gauss potential. Furthermore, as hypothesized in Sec. I, a plateau of $\approx 100\%$ recapture probabilities exists for repelling potentials. We see values of $\tau_{\text{recap,i-Gauss}}/\tau_{\text{recap,Free}} \approx 0.33$. When switching off

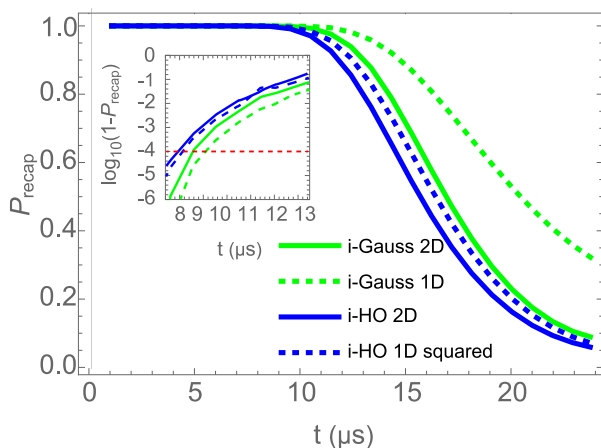


FIG. 8. Recapture probabilities for $U_0 = 50 \mu\text{K}$ and $\omega = 25 \text{ kHz}$ for two dimensions (radial) under the i-Gauss potential, together with the i-HO 2D lower bound and the i-HO 1D squared approximation. The dashed red line in the inset indicates the recapture probability bound for τ_{recap} . The i-HO 2D case is a lower bound for the i-Gauss 2D case, and the i-HO 1D case squared finely approximates the i-Gauss 2D case.

the traps, all atoms expand under the free potential, whereas when the traps are kept on, only the atom that has been excited to the Rydberg state will expand under the i-Gauss potential. These results then indicate that the overall heating would be significantly lower when the traps are kept on. The blinking heating and control issues, persisting when repeatedly switching the traps on and off, further support the strategy of leaving the traps on [12].

To further investigate this statement, we vary the trap parameters U_0 and ω and calculate $\tau_{\text{recap,i-Gauss}}$ and $\tau_{\text{recap,Free}}$. Note that $\omega \sim \sqrt{U_0}$, but we can independently vary U_0 and ω by varying the width of the laser w_0 as in Eq. (4). The results in Fig. 7 show that τ_{recap} increases with decreasing ω and with increasing U_0 . For ω , this behavior is logical as traps become tighter for increasing ω [see Eq. (4)], resulting in fewer bound states. For U_0 , the traps become deeper, resulting in faster expansion but also more bound states, which for this range of parameters seem to be the dominating factor. We see that the contour lines in Fig. 7(a) are approximately straight lines for our considered range of parameters. We can therefore take the trap edge X_{edge} of Eq. (8) to be a predictor of the recapture time τ_{recap} . Figure 7(b) shows the values of the ratio $\tau_{\text{recap,i-Gauss}}/\tau_{\text{recap,Free}}$ for the range of parameters, and we see that the values lie in the interval $[0.3, 0.6]$, indicating that the recapture times stay in the same order of magnitude.

Figure 8 shows the recapture probabilities for the 2D case compared to the squared 1D approximation. We see indeed that the squared 1D approximation follows the 2D recapture probability. As we are mostly interested in the point τ_{recap} , this approximation is satisfactory.

IV. CONCLUSION

This work outlined the development of a robust quantum-mechanical model for the calculation of recapture probabilities under various potentials. The squared recapture probabilities of a 1D i-HO potential (for which an analytical

expression exists) nicely approximate the 2D i-Gauss potential recapture probabilities. From the results in Sec. III, we see that for relevant trap parameters, the recapture time τ_{recap} is of the same order of magnitude under a free potential as under an i-Gauss potential. This indicates that for a large array of atoms, it is more beneficial to keep the traps on, thus heating up only a single atom, than to heat up the entire array when switching the traps off.

Future studies could incorporate other loss rates, such as blackbody radiation, stimulated emission in the Rydberg state, and trap scattering caused by off-resonant excitations. Furthermore, the consideration of reachable atom temperatures given the trap parameters U_0 and ω should be taken into account. A treatment of bottle beam traps [14] using this quantum-mechanical model would also be of great interest. Last, the 1 μK temperatures treated in this work are mostly relevant for Sr and Yb systems. In higher-temperature systems

(10 μK for Rb, Cs, etc.), often, higher values of ω are possible as well, leading to values of $Z_N/Z > 0.99$ of around $N = 9$ [40]. This would mean more terms are relevant in the sum of Eq. (6).

The data that support the findings of this study are available from the corresponding author upon reasonable request.

ACKNOWLEDGMENTS

We thank M. Mohan, D. J. van Rensburg, M. Venderbosch, J. Postema, L. Visser, and J. van de Kraats for fruitful discussions. This research is financially supported by the Dutch Ministry of Economic Affairs and Climate Policy (EZK) as part of the Quantum Delta NL program and by the Netherlands Organisation for Scientific Research (NWO) under Grant No. 680-92-18-05.

APPENDIX A: INTEGRALS

For the approximation of the bound states in Sec. II B, one needs to construct the matrix with matrix elements $\langle \psi_{\text{HO},n} | H_{\text{Gauss}} | \psi_{\text{HO},m} \rangle$. Numerical integration algorithms show significant errors at high values of n and m . Therefore, analytic expressions are used:

$$\begin{aligned} \langle \psi_{\text{HO},n} | H_{\text{Gauss}} | \psi_{\text{HO},m} \rangle &= \langle \psi_{\text{HO},n} | H_{\text{HO}} - \frac{1}{2}x^2 + V_{\text{Gauss}} | \psi_{\text{HO},m} \rangle \\ &= \langle \psi_{\text{HO},n} | H_{\text{HO}} | \psi_{\text{HO},m} \rangle - \langle \psi_{\text{HO},n} | \frac{1}{2}x^2 | \psi_{\text{HO},m} \rangle + \langle \psi_{\text{HO},n} | V_{\text{Gauss}} | \psi_{\text{HO},m} \rangle. \end{aligned}$$

The first two terms are fairly standard and can be found in most introductory quantum mechanics textbooks [33]. The last term involves terms of the form [41]

$$\int_{-\infty}^{\infty} e^{-ax^2} H_n(x) H_m(x) dx = \sqrt{\frac{\pi}{a}} n! m! \sum_{k=0}^{\min(n,m)} \frac{2^k (n+m-2k)!}{k!(n-k)!(m-k)! \left(\frac{n+m}{2} - k\right)!} \left(\frac{1-a}{a}\right)^{\frac{n+m}{2}-k}.$$

For the 2D case, the same decomposition is applied to calculate

$$\langle \psi_{\text{HO},n_1,l_1} | H_{\text{HO}} | \psi_{\text{HO},n_2,l_2} \rangle = (n_1 + 1) \delta_{n_1=n_2} \delta_{l_1=l_2}.$$

For the other two terms

$$\begin{aligned} \langle \psi_{\text{HO},n} | \frac{1}{2}r^2 | \psi_{\text{HO},m} \rangle &= C_0 \int_0^{2\pi} \int_0^{\infty} r e^{-\frac{r^2}{2}} r^{|l_1|} L_{\alpha_1}^{|l_1|}(r^2) e^{-l_1\phi} \frac{1}{2} r^2 e^{-\frac{r^2}{2}} r^{|l_2|} L_{\alpha_2}^{|l_2|}(r^2) e^{+il_2\phi} dr d\phi \\ &= \frac{1}{2} \pi C_0 \delta_{l_1=l_2} \int_0^{\infty} x^{\frac{|l_1|+|l_2|}{2}+1} e^{-x} L_{\alpha_1}^{|l_1|}(x) L_{\alpha_2}^{|l_2|}(x) dx, \\ \langle \psi_{\text{HO},n} | V_{\text{Gauss}} | \psi_{\text{HO},m} \rangle &= C_1 \int_0^{2\pi} \int_0^{\infty} r e^{-\frac{r^2}{2}} r^{|l_1|} L_{\alpha_1}^{|l_1|}(r^2) e^{-l_1\phi} \frac{U}{\hbar\omega} e^{\frac{1}{2}r^2 \frac{\hbar\omega}{U}} e^{-\frac{r^2}{2}} r^{|l_2|} L_{\alpha_2}^{|l_2|}(r^2) e^{+il_2\phi} dr d\phi \\ &= \pi C_1 \delta_{l_1=l_2} \int_0^{\infty} x^{\frac{|l_1|+|l_2|}{2}} e^{-x(1-\frac{\hbar\omega}{2U})} L_{\alpha_1}^{|l_1|}(x) L_{\alpha_2}^{|l_2|}(x) dx, \end{aligned}$$

where L_{α}^n is the generalized Laguerre polynomial, $C_i \in \mathbb{R}_+$ are normalization constants, and the substitution $r^2 \rightarrow x$ was made. These integrals can be calculated using the following identity [42]:

$$\int_0^{\infty} t^{\alpha-1} e^{-pt} L_m^{\lambda}(at) L_n^{\beta}(bt) dt = \frac{\Gamma(\alpha)(\lambda+1)_m(\beta+1)_n p^{-\alpha}}{m!n!} \sum_{j=0}^m \frac{(-m)_j (\alpha)_j}{(\lambda+1)_j j!} \left(\frac{a}{p}\right)^j \sum_{k=0}^n \frac{(-n)_k (j+\alpha)_k}{(\beta+1)_k k!} \left(\frac{b}{p}\right)^k. \quad (\text{A1})$$

Here, Γ is the gamma function, and $(a)_i$ is the Pochhammer symbol. Note that these symbols are highly discontinuous at negative integers. Therefore, sufficient care should be employed when calculating these expressions.

APPENDIX B: INITIAL QUANTUM SPREAD

We show the derivation of the expression of the initial quantum spread as in Eq. (8). Let l indicate a certain potential and consider the function

$$P_l(t) := |\langle \psi_0 | \psi_l(t) \rangle|^2.$$

In order to analyze its behavior, we need the following relations:

$$i\partial_t |\psi_l(t)\rangle = -\frac{1}{2} \frac{\partial^2}{\partial x^2} |\psi_l(t)\rangle + V_l |\psi_l(t)\rangle, \quad -\frac{1}{2} \frac{\partial^2}{\partial x^2} |\psi_0\rangle + V_l |\psi_0\rangle = E_0 |\psi_0\rangle.$$

The first derivative can be expressed as

$$\begin{aligned} \dot{P}_l(t) &= \overline{\langle \psi_0 | \partial_t \psi_l(t) \rangle} \langle \psi_0 | \psi_l(t) \rangle + \overline{\langle \psi_0 | \psi_l(t) \rangle} \langle \psi_0 | \partial_t \psi_l(t) \rangle \\ &= i \langle \psi_0 | -\frac{1}{2} \frac{\partial^2}{\partial x^2} + V_l | \psi_l(t) \rangle \langle \psi_0 | \psi_l(t) \rangle - i \overline{\langle \psi_0 | \psi_l(t) \rangle} \langle \psi_0 | -\frac{1}{2} \frac{\partial^2}{\partial x^2} + V_l | \psi_l(t) \rangle \\ &= i \left[\langle \psi_l(t) | -\frac{1}{2} \frac{\partial^2}{\partial x^2} + \frac{1}{2} x^2 | \psi_0 \rangle + \langle \psi_l(t) | V_l - \frac{1}{2} x^2 | \psi_0 \rangle \right] \langle \psi_0 | \psi_l(t) \rangle \\ &\quad - i \langle \psi_l(t) | \psi_0 \rangle \left[\langle \psi_0 | -\frac{1}{2} \frac{\partial^2}{\partial x^2} + \frac{1}{2} x^2 | \psi_l(t) \rangle + \langle \psi_0 | V_l - \frac{1}{2} x^2 | \psi_l(t) \rangle \right] \\ &= i \langle \psi_l(t) | E_0 | \psi_0 \rangle \langle \psi_0 | \psi_l(t) \rangle - i \langle \psi_l(t) | \psi_0 \rangle \langle \psi_0 | E_0 | \psi_l(t) \rangle + i \langle \psi_l(t) | \left[V_l - \frac{1}{2} x^2, | \psi_0 \rangle \langle \psi_0 | \right] | \psi_l(t) \rangle \\ &= i \langle \psi_l(t) | \left[V_l - \frac{1}{2} x^2, | \psi_0 \rangle \langle \psi_0 | \right] | \psi_l(t) \rangle. \end{aligned}$$

Note that at $t = 0$ this object is always equal to zero. For the second derivative, we get

$$\begin{aligned} \ddot{P}_l(t) &= i \langle \partial_t \psi_l(t) | \left[V_l - \frac{1}{2} x^2, | \psi_0 \rangle \langle \psi_0 | \right] | \psi_l(t) \rangle + i \langle \psi_l(t) | \left[V_l - \frac{1}{2} x^2, | \psi_0 \rangle \langle \psi_0 | \right] | \partial_t \psi_l(t) \rangle \\ &= i \langle \psi_l(t) | \left(\frac{1}{2} \frac{\partial^2}{\partial x^2} - V_l \right) \left[V_l - \frac{1}{2} x^2, | \psi_0 \rangle \langle \psi_0 | \right] | \psi_l(t) \rangle - i \langle \psi_l(t) | \left[V_l - \frac{1}{2} x^2, | \psi_0 \rangle \langle \psi_0 | \right] \left(\frac{1}{2} \frac{\partial^2}{\partial x^2} - V_l \right) | \psi_l(t) \rangle \\ &= i \langle \psi_l(t) | \left[\frac{1}{2} \frac{\partial^2}{\partial x^2} - V_l, \left[V_l - \frac{1}{2} x^2, | \psi_0 \rangle \langle \psi_0 | \right] \right] | \psi_l(t) \rangle. \end{aligned}$$

Looking at $t = 0$, we get

$$\begin{aligned} \ddot{P}_l(0) &= i \langle \psi_0 | \left(\frac{1}{2} \frac{\partial^2}{\partial x^2} - V_l \right) \left[\left(V_l - \frac{1}{2} x^2 \right) | \psi_0 \rangle \langle \psi_0 | - | \psi_0 \rangle \langle \psi_0 | \left(V_l - \frac{1}{2} x^2 \right) \right] \\ &\quad - \left[\left(V_l - \frac{1}{2} x^2 \right) | \psi_0 \rangle \langle \psi_0 | - | \psi_0 \rangle \langle \psi_0 | \left(V_l - \frac{1}{2} x^2 \right) \right] \left(\frac{1}{2} \frac{\partial^2}{\partial x^2} - V_l \right) | \psi_0 \rangle \\ &= \langle \psi_0 | \left(\frac{1}{2} \frac{\partial^2}{\partial x^2} - V_l \right) \left(V_l - \frac{1}{2} x^2 \right) | \psi_0 \rangle - \langle \psi_0 | \left(\frac{1}{2} \frac{\partial^2}{\partial x^2} - V_l \right) | \psi_0 \rangle \langle \psi_0 | \left(V_l - \frac{1}{2} x^2 \right) | \psi_0 \rangle \\ &\quad - \langle \psi_0 | \left(V_l - \frac{1}{2} x^2 \right) | \psi_0 \rangle \langle \psi_0 | \left(\frac{1}{2} \frac{\partial^2}{\partial x^2} - V_l \right) | \psi_0 \rangle + \langle \psi_0 | \left(V_l - \frac{1}{2} x^2 \right) \left(\frac{1}{2} \frac{\partial^2}{\partial x^2} - V_l \right) | \psi_0 \rangle \\ &= -2 \langle \psi_0 | V_l^2 | \psi_0 \rangle + 2 \langle \psi_0 | V_l | \psi_0 \rangle^2 + 2 \langle \psi_0 | V_l \frac{1}{2} \frac{\partial^2}{\partial x^2} | \psi_0 \rangle + 2 \langle \psi_0 | \frac{1}{2} x^2 V_l | \psi_0 \rangle + 2 \langle \psi_0 | -\frac{1}{4} x^2 \frac{\partial^2}{\partial x^2} | \psi_0 \rangle \\ &\quad + 2 \langle \psi_0 | \frac{1}{2} x^2 | \psi_0 \rangle \langle \psi_0 | \frac{1}{2} \frac{\partial^2}{\partial x^2} | \psi_0 \rangle - 2 \langle \psi_0 | \frac{1}{2} x^2 | \psi_0 \rangle \langle \psi_0 | V_l | \psi_0 \rangle \\ &\quad - 2 \langle \psi_0 | V_l | \psi_0 \rangle \langle \psi_0 | \frac{1}{2} \frac{\partial^2}{\partial x^2} | \psi_0 \rangle + \langle \psi_0 | \frac{1}{2} \frac{\partial^2}{\partial x^2} V_l | \psi_0 \rangle - \langle \psi_0 | \frac{1}{2} | \psi_0 \rangle - 2 \langle \psi_0 | V_l^2 | \psi_0 \rangle + 2 \langle \psi_0 | V_l | \psi_0 \rangle^2 \\ &= 2 \left(\frac{1}{2} \langle \psi_0 | \left\{ \frac{1}{2} \frac{\partial^2}{\partial x^2} + \frac{1}{2} x^2, V_l \right\} | \psi_0 \rangle - \langle \psi_0 | \frac{1}{2} \frac{\partial^2}{\partial x^2} + \frac{1}{2} x^2 | \psi_0 \rangle \langle \psi_0 | V_l | \psi_0 \rangle \right) \\ &\quad + 2 \left(\frac{1}{2} \langle \psi_0 | \left\{ \frac{1}{2} \frac{\partial^2}{\partial x^2}, -\frac{1}{2} x^2 \right\} | \psi_0 \rangle - \langle \psi_0 | \frac{1}{2} \frac{\partial^2}{\partial x^2} | \psi_0 \rangle \langle \psi_0 | -\frac{1}{2} x^2 | \psi_0 \rangle \right). \end{aligned}$$

We define

$$\begin{aligned}\text{Var}_\psi(A) &:= \langle \psi | A^2 | \psi \rangle - \langle \psi | A | \psi \rangle^2, \\ \text{Cov}_\psi(A, B) &:= \frac{1}{2} \langle \psi | \{A, B\} | \psi \rangle - \langle \psi | A | \psi \rangle \langle \psi | B | \psi \rangle\end{aligned}$$

and note that $\text{Cov}_\psi(A, A) = \text{Var}_\psi(A)$. We then have

$$\ddot{P}_l(0) = -2\text{Var}_{\psi_0}(V_l) + 2\text{Cov}_{\psi_0}\left(\frac{1}{2}\frac{\partial^2}{\partial x^2} + \frac{1}{2}x^2, V_l\right) - 2\text{Cov}_{\psi_0}\left(\frac{1}{2}\frac{\partial^2}{\partial x^2}, \frac{1}{2}x^2\right).$$

Using the linearity of the covariance, we can also write this as

$$\ddot{P}_l(0) = -2\text{Cov}_{\psi_0}\left(V_l - \frac{1}{2}\frac{\partial^2}{\partial x^2}, V_l - \frac{1}{2}x^2\right).$$

We can now calculate this term for the i-HO and i-Gauss potentials, with $|\psi_0\rangle$ being the HO ground state, to get $\ddot{P}_{\text{init, i-HO}}(0) = -1$ and $\ddot{P}_{\text{init, i-Gauss}}(0) = -0.98$ ($U_0 = 50 \mu\text{K}$ and $\omega = 25 \text{ kHz}$), indicating faster decay for i-HO than for i-Gauss.

-
- [1] A. W. Young, W. J. Eckner, W. R. Milner, D. Kedar, M. A. Norcia, E. Oelker, N. Schine, J. Ye, and A. M. Kaufman, *Nature (London)* **588**, 408 (2020).
- [2] I. Cong, N. Maskara, M. C. Tran, H. Pichler, G. Semeghini, S. F. Yelin, S. Choi, and M. D. Lukin, [arXiv:2209.12428](https://arxiv.org/abs/2209.12428).
- [3] M. Saffman, *J. Phys. B* **49**, 202001 (2016).
- [4] D. S. Weiss and M. Saffman, *Phys. Today* **70**(7), 44 (2017).
- [5] X. Wu, X. Liang, Y. Tian, F. Yang, C. Chen, Y.-C. Liu, M. K. Tey, and L. You, *Chin. Phys. B* **30**, 020305 (2021).
- [6] T. Topcu and A. Derevianko, [arXiv:1505.07152](https://arxiv.org/abs/1505.07152).
- [7] M. Mohan, R. de Keijzer, and S. Kokkelmans, *Phys. Rev. Res.* **5**, 033052 (2023).
- [8] O. Man'ko and V. Man'ko, *J. Russ. Laser Res.* **20**, 67 (1999).
- [9] R. de Keijzer, O. Tse, and S. Kokkelmans, *Quantum* **7**, 908 (2023).
- [10] S. Jandura, J. D. Thompson, and G. Pupillo, *PRX Quantum* **4**, 020336 (2023).
- [11] I. S. Madjarov, J. P. Covey, A. L. Shaw, J. Choi, A. Kale, A. Cooper, H. Pichler, V. Schkolnik, J. R. Williams, and M. Endres, *Nat. Phys.* **16**, 857 (2020).
- [12] I. Madjarov, Entangling, controlling, and detecting individual strontium atoms in optical tweezer arrays, Ph.D. thesis, Caltech University, 2021.
- [13] S. M. Blinder, *J. Math. Phys.* **25**, 905 (1984).
- [14] D. Barredo, V. Lienhard, P. Scholl, S. de Léséleuc, T. Boulier, A. Browaeys, and T. Lahaye, *Phys. Rev. Lett.* **124**, 023201 (2020).
- [15] A. Pagano, S. Weber, D. Jaschke, T. Pfau, F. Meinert, S. Montangero, and H. P. Buchler, *Phys. Rev. Res.* **4**, 033019 (2022).
- [16] D. Bluvstein, H. Levine, G. Semeghini, T. T. Wang, S. Ebadi, M. Kalinowski, A. Keesling, N. Maskara, H. Pichler, M. Greiner, V. Vuletić, and M. D. Lukin, *Nature (London)* **604**, 451 (2022).
- [17] M. Endres, A. Cooper-Roy, J. P. Covey, I. S. Madjarov, A. L. Shaw, V. Schkolnik, J. R. Williams, and J. Choi, [Controlling, detecting and entangling alkaline-earth Rydberg atoms in tweezer arrays](https://arxiv.org/abs/20220238245A1), U.S. Patent No. 20220238245A1 (2022).
- [18] C. Tuchendler, A. M. Lance, A. Browaeys, Y. R. P. Sortais, and P. Grangier, *Phys. Rev. A* **78**, 033425 (2008).
- [19] P. D. Lett, R. N. Watts, C. I. Westbrook, W. D. Phillips, P. L. Gould, and H. J. Metcalf, *Phys. Rev. Lett.* **61**, 169 (1988).
- [20] J. P. Covey, I. S. Madjarov, A. Cooper, and M. Endres, *Phys. Rev. Lett.* **122**, 173201 (2019).
- [21] T. Akatsuka, M. Takamoto, and H. Katori, *Phys. Rev. A* **81**, 023402 (2010).
- [22] C. Zhang, F. Pokorny, W. Li, G. Higgins, A. Pöschl, I. Lesanovsky, and M. Henrich, *Nature (London)* **580**, 345 (2020).
- [23] S.-K. Chu, C.-T. Ma, R.-X. Miao, and C.-H. Wu, *Ann. Phys. (NY)* **395**, 183 (2018).
- [24] J. Alda, *Encyclopedia of Optical Engineering* (Marcel Dekker Inc., New York, 2003), p. 999.
- [25] M. S. Safronova, U. I. Safronova, and C. W. Clark, *Phys. Rev. A* **94**, 012505 (2016).
- [26] In this work, the PYTHON library ARC3.0 was used for polarizability calculations [43].
- [27] M. S. Safronova, S. G. Porsev, U. I. Safronova, M. G. Kozlov, and C. W. Clark, *Phys. Rev. A* **87**, 012509 (2013).
- [28] A. Cooper, J. P. Covey, I. S. Madjarov, S. G. Porsev, M. S. Safronova, and M. Endres, *Phys. Rev. X* **8**, 041055 (2018).
- [29] J. D. Thompson, T. G. Tiecke, A. S. Zibrov, V. Vuletić, and M. D. Lukin, *Phys. Rev. Lett.* **110**, 133001 (2013).
- [30] A. M. Kaufman, B. J. Lester, and C. A. Regal, *Phys. Rev. X* **2**, 041014 (2012).
- [31] S. Nandi, *Am. J. Phys.* **78**, 1341 (2010).
- [32] M. Cohen, *J. Phys. A* **17**, L101 (1984).
- [33] D. J. Griffiths, *Introduction to Quantum Mechanics*, 2nd ed. (Pearson Prentice Hall, Upper Saddle River, New Jersey, 2004).
- [34] P. A. Golovinski, [arXiv:1905.04591](https://arxiv.org/abs/1905.04591).
- [35] P. Pfeifer, *Phys. Rev. Lett.* **70**, 3365 (1993).
- [36] S. Luo, *J. Phys. A* **38**, 2991 (2005).
- [37] C. Sheng, X. He, P. Xu, R. Guo, K. Wang, Z. Xiong, M. Liu, J. Wang, and M. Zhan, *Phys. Rev. Lett.* **121**, 240501 (2018).
- [38] H. Levine, A. Keesling, G. Semeghini, A. Omran, T. T. Wang, S. Ebadi, H. Bernien, M. Greiner, V. Vuletić, H. Pichler, and M. D. Lukin, *Phys. Rev. Lett.* **123**, 170503 (2019).
- [39] J. C. Butcher, Numerical differential equation methods, in *Numerical Methods for Ordinary Differential Equations* (Wiley, Hoboken, NJ, 2016), Chap. 2, pp. 55–142.

- [40] H. Bernien, S. Schwartz, A. Keesling, H. Levine, A. Omran, H. Pichler, S. Choi, A. S. Zibrov, M. Endres, M. Greiner, V. Vuletić, and M. D. Lukin, *Nature (London)* **551**, 579 (2017).
- [41] W. N. Bailey, *J. London Math. Soc.* **s1-23**, 291 (1948).
- [42] L. Poh-aun, S. Ong, and H. M. Srivastava, *Int. J. Comput. Math.* **78**, 303 (2001).
- [43] E. Robertson, N. Šibalić, R. Potvliege, and M. Jones, *Comput. Phys. Commun.* **261**, 107814 (2021).